Available online at www.sciencedirect.com
SCIENCE DIRECT
Polymer 46 (2005) 11003–11018
polymer
www.elsevier.com/locate/polymer

A comparison of computer models for the simulation of crystalline polyethylene and the long *n*-alkanes.

T.L. Phillips, S. Hanna*

H. H. Wills Physics Department, University of Bristol, Tyndall Avenue, Bristol BS8 1TL, UK

Received 23 March 2005; received in revised form 3 September 2005; accepted 5 September 2005
Available online 3 October 2005

Abstract

We address the problem of simulating the orthorhombic crystal structures of polyethylene (PE) and the long *n*-alkanes. Experimentally, the lattice parameters of these materials are known to depend on the level of disorder in the crystals. This introduces complications when developing reliable force field parameters for computer models. In this paper we compare the behaviours of three different atomistic computer models, which possess varying degrees of disorder. The first model consists of chains, which are infinite, by virtue of the periodic repeat of the simulation cell along the chain axis. The second model consists of finite chain stems, whose lengths are determined by the z-dimension of the simulation box. The third model, known as the jogged chain model, attempts to reproduce the effect of defects and chain folds, by allowing a finite chain to pass through the simulation box more than once. Jogs are introduced into each chain, preventing it from intersecting with periodic images of itself. The same force field parameters are used in each case. For the force field chosen, it is found that the jogged chain model provides a better match with the *a*-parameter of the experimental unit cell of PE than the other two models. In the infinite and finite chain models, it is found that the chains librate as rigid rotors and the formation of dynamic defects is rare. On the other hand, the extra free volume resulting from the defects in the jogged chain model, means that *gauche* defects form readily in this case. We conclude that, for the force field chosen, the jogged chain model is better suited to the simulation of chain-folded PE crystals than the more ordered models. Our results are compared with experimental results and previous simulations of PE from the literature.
© 2005 Elsevier Ltd. All rights reserved.

Keywords: Polyethylene; Computer simulation; Orthorhombic phase

1. Introduction

In this paper we address the problem of simulating crystalline polyethylene (PE) and the long *n*-alkanes. We compare and contrast three computer models designed for the purpose, highlighting the successes and deficiencies of each.

PE exists in three distinct crystalline forms. At ambient temperature and pressure, the crystal structure is orthorhombic. The polymer chains consist of long *trans*-sequences of carbon atoms which form planar zig-zags that pack in a herringbone arrangement [1–4] (Fig. 1). The lattice parameters and thermal expansion behaviour of PE have been investigated by many previous workers (for example Refs. [5–9]). It is found that most thermal expansion occurs parallel to the *a*-axis of the unit cell, and that there is some contraction with increasing temperature parallel to the *c*-axis, which coincides with the chain axis. It has also been established that the lattice parameters are dependent on the presence of crystal defects. In particular the presence of chain folds influences the chain packing, so that the crystal density varies with the distance between fold surfaces [8]. A similar effect has been reported in the ultra-long *n*-alkanes [10]. As a consequence it is observed that the lattice parameters of orthorhombic, chain-folded PE crystals depend on the crystallisation temperature and annealing history of the sample.

The chain setting angle, i.e. the angle between the plane of the polymer backbone and the *a*-axis (marked in Fig. 1), is an important structural parameter which has been reported in many investigations [3,11–16]. As with the lattice parameters, the setting angle is also influenced by temperature and the presence of defects [12]. Currently accepted values lie in the range 42–46° [17].

Two other crystal forms of PE are also observed. The first is a monoclinic crystal form, which can arise when a stress is applied to the sample. In this phase, the chains still consist of *trans*-sequences, but the planes of the zig-zags stack in a parallel fashion within the unit cell [18–20]. In this paper we

* Corresponding author. Tel.: +44 117 928 8771; fax: +44 117 925 5624.
E-mail address: s.hanna@bristol.ac.uk (S. Hanna).

0032-3861/$ - see front matter © 2005 Elsevier Ltd. All rights reserved.
doi:10.1016/j.polymer.2005.09.040

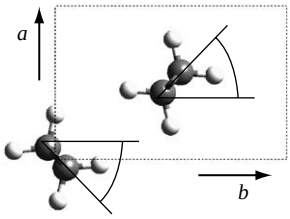

Fig. 1. The crystalline unit cell for polyethylene and long *n*-alkanes, viewed down the chain axis (*c*-axis). The marked angles are the setting angles of the polymer chains. The setting angle is taken as positive for angles increasing in a clockwise sense.

will use the term monoclinic packing to indicate when regions of adjacent chain stems have the same setting angles. The second phase is a hexagonal phase which is found at high pressure and temperature [21–23]. In this phase, the polymer chains partially collapse in the chain axis direction as kinks form in the backbone, and the packing of the chain stems transforms to that of cylinders. Any registration of the polymer chains parallel to the *c*-axis is lost. In this form the chains slide rapidly along their lengths, leading to crystal thickening and ultimately chain-extended crystals. The hexagonal phase is not accessible at ambient pressure.

One of the difficulties in constructing a computer model of a PE crystal, is that the model needs to be very large if it is to encompass all of the structural features present in a real system. PE normally crystallises in a chain-folded morphology, with the distance between fold surfaces typically being in the region of 10–20 nm. This implies a polymer backbone length (or chain stem length) of *c*. 80–160 carbon atoms between the fold surfaces, so that the model quickly becomes prohibitively large if a reasonable number of chain stems are included in the simulation. However, as described above, the presence of fold surfaces, and other defects, significantly affects the lateral packing of the chain stems, so that it is important for any realistic computer model to take these influences into account.

When developing a model for crystalline PE, the *n*-alkanes might appear to offer a convenient starting point. Since any computer model is limited in size by the available computing resources, a system consisting of short PE-like chain segments packed in a crystal would appear advantageous. However, it is observed experimentally that the crystal structures of the shorter *n*-alkanes (i.e. $C_{33}H_{68}$ and below) depend on the chain length and temperature. On heating, instead of a single orthorhombic phase, these short-chain crystals may pass through several other crystal or plastic crystal phases before melting occurs [24,25]. The differences between the various phases arise from the packing of the chain ends, which lead to different lateral packing arrangements, and the tilting of the chains. The rotator phases of the *n*-alkanes have formed the basis of a number of interesting simulation studies (e.g. Refs. [26–29]). Simulations of the orthorhombic phases of short *n*-alkanes have been reported by McGann and Lacks [30] and Mavrantza et al. [31]. In both cases, a dependence of cell density on the length of chain simulated was reported. Thus, although the short *n*-alkanes are interesting materials in their own right, they are far from ideal as models for PE.

At the other extreme of molecular length, it is possible to simulate a pseudoinfinite PE chain, by using periodic boundary conditions and covalently bonding the chain stems across the ends of the simulation box. Using such a model, Ryckaert and Klein were able to reproduce the lattice parameters of the *n*-alkanes very well [32]. However, they failed to reproduce the higher temperature hexagonal or rotator phases, and their model suffered from excessive longitudinal diffusion of the chain stems. Other simulations based on the infinite chain model have been presented more recently [31,33,34]. Although the infinite chain model might be considered a useful model for extended chain crystals, it appears that the tight constraints placed on the chains by the boundary conditions will tend to limit the formation of conformational defects: the contraction of one chain relative to its neighbours is strongly inhibited, because the periodic bonding prevents any one chain from being shorter in the *c* direction than the others. This will, of course, limit the usefulness of the model at higher temperatures.

Therefore, despite the fact that they are frequently cited in the literature, it appears that models based on either infinite chains or short *n*-alkanes cannot be expected to reproduce the structure and phase behaviour of PE reliably.

An interesting compromise between these two modelling extremes, is to consider modelling the ‘long’ *n*-alkanes. We will take ‘long’ in this context to refer to *n*-alkanes with 100 or more backbone carbon atoms. The long *n*-alkanes form ideal model materials, because the chain stems are sufficiently long that they provide a well-ordered representation of the PE unit cell, while at the same time they form crystals with a tightly regulated distance between folds. The materials, which include $C_{102}H_{206}$, $C_{198}H_{398}$ and $C_{390}H_{782}$, have formed the basis of several interesting experimental investigations in recent years (e.g. Refs. [10,35–37]). Computer models of long *n*-alkane crystals were considered by Wunderlich and co-workers. Their models consisted of clusters of chain stems containing 50 or 100 CH_2 units [38–40]. In the models, each CH_2 unit was replaced by a single united atom, and free boundary conditions were used, producing a small crystallite in a vacuum. The lack of boundary conditions and use of united atoms were probably major factors that prevented the room temperature structure of polyethylene from being reproduced. It is now recognised that PE cannot be modelled accurately using a united atom potential, and attention has turned to performing realistic all-atom simulations [31,41,42].

In the present paper, we aim to compare the predictions of three different atomistic models for the structures and dynamic properties of PE at different temperatures. The models all consist of simulation boxes that are small compared with the dimensions of a chain-folded crystal. However, by incorporating different levels of disorder, we will show that it is possible to simulate the characteristics of real PE crystals, as well as of the more ordered long *n*-alkanes. Although the three models are structurally different, the same molecular mechanics force field is used, so that any differences in behaviour may be attributed to the types of defects present in each case. The first two models consist of conventional finite and infinite chain

representations, as discussed above. However, the third model consists of finite chains that are longer than the simulation box, and which pass through the box more than once. In order to avoid self-intersection, each chain contains a jog defect; the defects are arranged randomly throughout the simulation cell to avoid an excessive build-up of strain. The jog defects are just one example of the types of defects which might be expected in real PE crystals, others include chain-folds, kinks, branch points and chain-ends, and it is anticipated that their inclusion will bring our model a step closer to reality. In fact, we will show that the inclusion of jog defects leads to a similar expansion of the unit cell as might be expected from the presence of chain-folds. For a given choice of force field, we will also demonstrate that wide variations in structural parameters and dynamic behaviour are possible, depending on the choice of model.

2. Models and methods

2.1. Choice of model

Three model systems have been simulated: an infinite chain model, a finite chain model, and a jogged chain model (see previous paragraph). All models make use of periodic boundary conditions. In the infinite chain model, each chain stem is covalently bonded across the (001) face of the unit cell, effectively forming an infinite polymer chain. The starting point for the infinite chain model was derived from an array of $4\times6\times24$ unit cells of PE, and thus, consists of 48 chain stems each of 48 carbon atoms (Fig. 2(a)). The finite chain model was similar in construction to the infinite chain model and consisted of an array of 48 $C_{48}H_{98}$ molecules.

The third computer model was inspired by the ultra-long *n*-alkanes which were discussed above, and which were developed for use as experimental models for PE. Our initial thought was that a model based on these materials would, similarly, provide a useful computational representation of a real PE crystal. The computer model was based on molecules of $C_{102}H_{206}$, which normally crystallises in chain extended form, but which has a molecular length comparable to the length of the chain stems in chain folded PE crystals.

A model containing 48 fully extended $C_{102}H_{206}$ molecules would have an aspect ratio (length:width), of *c*. 4:1. For technical reasons (see below) this model is not stable under the molecular dynamics implementation that we are using. Therefore, an alternative approach is required.

In our modified model for $C_{102}H_{206}$ the chains cross the periodic boundary twice, facilitated by a jog defect (Fig. 3(a)). By including a jog in each chain, one chain can occupy two chain stem sites and, under periodic boundary conditions, the simulation box will have an aspect ratio of only 2:1. In this system there are 48 chain stems but only 24 chains. The resulting model is rich in defects in the form of jogs and chain ends. It allows the study of the conformations and dynamics of a significant number of jog defects and chain ends over a range of temperatures while, at the same time, providing a more PE-like environment within the constraints of the simulation

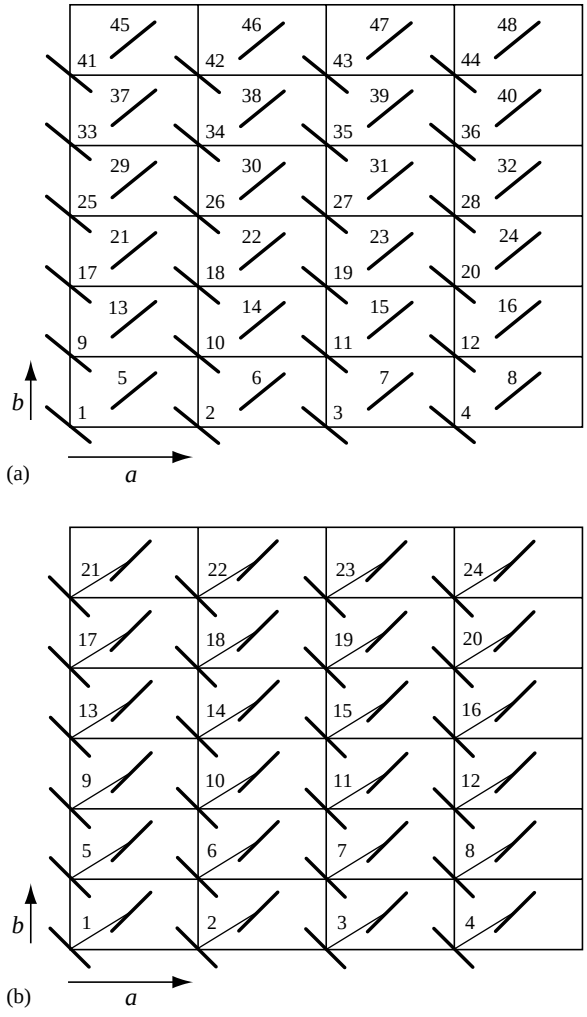

Fig. 2. (a) The ordering of chain stems within the simulation box for the finite and infinite chain models. (b) The ordering of chain stems within the simulation box for the $4\times6\times C_{102}$ jogged chain model. The views are taken looking down the *c*-axis of the unit cell.

method and current computing resources. However, the model is no longer an accurate representation of the $C_{102}H_{206}$ crystal that was its inspiration. A plan of the starting configuration is shown in Fig. 2(b); a three-dimensional view is given in Fig. 3(b).

A summary of model types, descriptions and compositions used in this paper is given in Table 1. The convention used in describing the models is as follows: 4×6 indicates four unit cells of PE in the *a* direction and six in the *b* direction; the use of 24 indicates the number of PE unit cells in the *c* direction for infinite chain models, while C_{48} and C_{102} indicate the length of the carbon backbone for the finite chain and jogged chain models, respectively.

2.2. Model construction

Models were constructed using the coordinates of the carbon atoms given for the PE unit cell by Bunn [2] ($a=0.740$ nm, $b=0.493$ nm, $c=0.2534$ nm). The positions of the hydrogen atoms were determined by minimising the potential

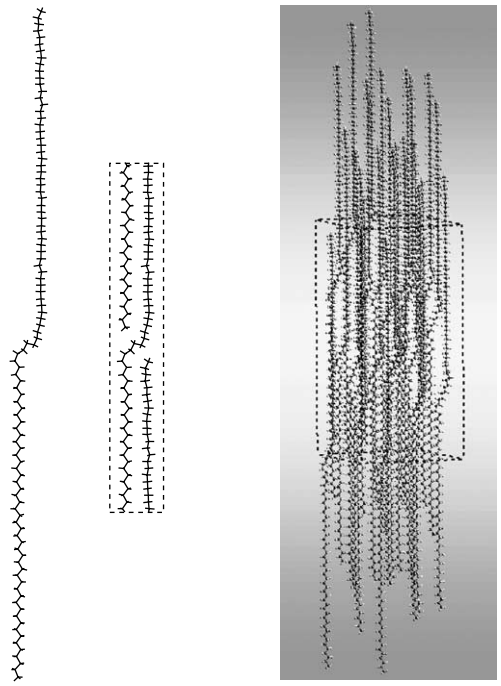

(a) (b)

Fig. 3. (a) The jogged chain motif used to build the jogged chain model. The motif is shown (left) as an isolated chain and (right) within a periodic bounding box. (b) A typical starting configuration of the jogged chain model.

energies of the completed models, keeping the cell dimensions fixed. The infinite chain models were constructed by repeated duplication of the Bunn unit cell in the *a*, *b* and *c* directions. The finite extended chain models were constructed from the infinite chain models, by cutting the bond across the (001) face of the simulation box and adding hydrogen atoms to the terminal CH_2 groups. The energy of the model was then minimised, in order to adjust the packing of the chain ends in the *c* direction.

The jogged chain models were built using the PE unit cell to construct a pair of chain stems, one at the corner of the cell, and the other at the centre. The periodic boundary conditions were then removed and short sections from the middle of the chain stems deleted. A jog defect was formed by joining parts of the two different stems, and the remaining ends were converted to CH_3 groups. The energy of the structure was then minimised. This $C_{102}H_{206}$ looped-chain, containing a single jog, provided a motif to build the model structure. By systematically repeating the motif in the *a* and *b* directions and randomly displacing it by an integer number of PE unit cells in the *c* direction—to avoid formation of a defect plane (Fig. 3(b))—a model consisting of 4×6 jogged-chain motifs was constructed.

Table 1
A summary of the model types and chain compositions used in the current study

Model	Chain type	Number of chains	Number of atoms
$4\times6\times24$ (infinite)	$-C_{48}H_{96}-$	48	6912
$4\times6\times C_{48}$ (finite)	$C_{48}H_{98}$	48	7008
$4\times6\times C_{102}$ (jogged)	$C_{102}H_{206}$	24	7392

For all models, the dimensions of the simulation box were approximately $30\times30\times60$ Å at ambient temperature and pressure.

2.3. Molecular dynamics method

Molecular dynamics simulations were performed using the DL_POLY_2 molecular dynamics code from the CCLRC [43]. All simulations were performed using a four processor Silicon Graphics Origin 200 computer. Models were equilibrated at constant temperature and pressure using the Berendsen method [44]. Equilibration was continued until any systematic variations in the simulation cell dimensions appeared to have relaxed. Simulations were performed at 300 and 400 K and ambient pressure for the $4\times6\times24$ infinite chain model and the $4\times6\times C_{48}$ finite chain model, and at a range of temperatures between 200 and 420 K for the $4\times6\times C_{102}$ jogged chain model, as detailed in Table 2. A production period of 50 ps was deemed sufficient to sample the dynamics of each system. A 1 fs time-step was used.

For equilibration, the Berendsen approach to isobaric–isothermal simulation was preferred over the Nosé–Hoover method [45,46], because it was more efficient at redistributing the thermal energy between the different vibrational modes of the system. This was a particular issue in the current simulations due to the anisotropic nature of the PE crystal; the vibrational modes along the chain axis have a considerably higher velocity than those oscillating normal to the chain direction. The Berendsen method cannot be used to calculate thermodynamic functions of the system, because it does not sample the isobaric–isothermal ensemble correctly. To overcome this shortcoming, all sampling was performed, after equilibration, in the microcanonical (constant NVE) ensemble.

The Berendsen method has two parameters, τ_T and τ_P, that control the coupling of the system to the temperature and pressure reservoirs. τ_T was set to 0.4 ps as suggested by Berendsen et al. [44]. The choice of τ_P required some care. It was found that if too short a time constant were chosen then the molecular dynamics algorithm became unstable. This was a consequence of the anisotropy both in the dimensions of the simulation box and in the compressibility of the system.

Table 2
A summary of the simulations presented in the present study

Model	*T* (K)	Equilibration period (ps)	Production period (ps)
$4\times6\times24$ (infinite)	300	200	50
	400	100	50
$4\times6\times C_{48}$ (finite)	300	100	50
	400	400	50
$4\times6\times C_{102}$ (jogged)	200	100	50
	300	100	50
	320	100	50
	340	100	50
	360	100	50
	380	100	50
	400	100	50
	420	100	50

The overall effect is that the SHAKE algorithm, used to maintain constant bond lengths (see below) will occasionally fail to converge. The likelihood of failure increases with the anisotropy of the system. This problem was overcome in two ways. Firstly, τ_P was given a large value (8 ps), which reduced the rate of change of the box dimensions, at the cost of slower equilibration, and secondly, the aspect ratio of the simulation box was limited to 2:1 or less. With these provisos, the stability of the method could be guaranteed at ambient pressures, and at temperatures below the experimentally determined melting points. Typically, when simulating crystalline systems of around 7000 atoms, the temperature was found to be constrained to within ± 5 K and the pressure to ± 0.5 kbar.

2.4. Force field

In selecting a suitable force field for the simulations, the first choice to be made is between a united atom representation, in which the hydrogen atoms are subsumed into the carbon atoms, and an all-atom representation, where all of the hydrogen atoms are explicitly modelled. Earlier investigations have indicated that the united atom approximation does not provide a good representation of the crystal structures of alkanes [47]. Our own experience in applying such a force field to the infinite PE model was that it resulted in a mobile hexagonal phase at room temperature. This finding is clearly at odds with experimental expectations, and is a consequence of the lack of detail in the united atom potential. For this reason, an all-atom force field has been used throughout this work, even though this leads to an order of magnitude increase in the processor time required compared to the united atom case.

A number of research groups have developed detailed all-atom force fields for the *n*-alkanes. Some examples include the MM4 [48], KGD [49] and SDFF [50] force fields. We have used a force field derived by Smith and Yoon [51] for the present study. This force field was chosen because its authors placed a strong emphasis on determining the correct form for the backbone torsional potential. The torsional potential is a key factor in reproducing both the static structure and dynamic motion of non-planar chain conformations. It is thus, crucial to the accurate modelling of the formation of gauche defects in PE crystals at high temperatures. This requirement should be contrasted with studies of sub-ambient-temperature PE crystals, in which the chains do not deviate significantly from the *trans* torsional state, and the role of the torsional potential is less significant [34,52]. It is perhaps worth noting, that the Smith and Yoon force field was designed for studying amorphous polymers, so that we might expect it to provide a good representation of *gauche* defects in more regular systems.

The potential forms and parameters for the force field are taken from Table 1 of Ref. [51]. The van derWaals interaction is represented by an 'Exponential 6' or Buckingham potential, with a relatively short cut-off length of 6 Å. A long-range correction to the pressure was employed. Energy terms are calculated for all pairs of atoms separated by three or more bonds. The lengths of all bonds are held constant using the SHAKE algorithm [47,53]. The torsional potential was designed to model the behaviour of *n*-butane. The parameters given by Smith and Yoon yield a *trans–gauche* energy difference of 2.0 kJ mol^{-1}, and a *trans–gauche* barrier of 12.6 kJ mol^{-1}. The *cis* barrier is 20.2 kJ mol^{-1} and the energy barrier for methyl group rotation is 10.9 kJ mol^{-1} [51].

The Smith and Yoon force field reproduces the structural and dynamic properties of *n*-alkane melts very well [51,54,55], but was not designed to reproduce the vibrational characteristics of *n*-alkane crystals. Thus, it may not produce such accurate results as the more detailed force field of Dasgupta et al. [49]. However, the Smith and Yoon force field was chosen for the present work because it provides a useful compromise between accuracy and computational effort for these polyethylene-like systems.

2.5. Analysis of torsional angles

The torsional angles in alkane chains determine the overall shape of the chains. Within a crystal the majority of the chains will be planar zig-zags with all of the torsional angles in the *trans* state. However, conformational defects can also form spontaneously within a crystal lattice when one or more torsional angles move to either the *gauche*$^+$ or *gauche*$^-$ potential minimum. It is instructive, therefore, to examine distributions of torsional angles for each system simulated. It is also enlightening to study the progress of individual torsional angles and defects. Using an enhanced form of a method presented by Doherty and Hopfinger [56], it is possible to visualise all of the torsional angles within a chain stem, as a function of time, in a two dimensional map. By plotting the position of each torsional conformation within the model against the *y*-axis and by indicating the angle by a block of colour, a single vertical line of colours can indicate the torsional angles of the whole chain stem. As one vertical line of colour indicates the state of the torsional angles at one point in time, a succession of such lines can show the evolution of the torsional states of the model with time. There is a simple mapping between the positions of the torsional angles within the chain stem and in the colour map. The colour map is shown in Fig. 4(a), and the colour table used to represent the angles in Fig. 4(b). The colours have been selected in such a way as to give a clear colour difference between the different conformational states. The trans conformation is green, while the *gauche*$^+$ and *gauche*$^-$ conformations are blue and red, respectively. The transition from *trans* to *gauche*$^+$ is achieved via turquoise, while a similar transition to *gauche*$^-$ is via yellow.

2.6. Analysis of setting angles

The same method that is used to visualise the evolution of the torsional angles can be used to look at the setting angles of the chains, either for whole chains or small sub-units of the chains. The sub-unit that has been chosen consists of three consecutive methylene groups or carbon atoms. The setting angle of this three-methylene-segment (3MS) is obtained by

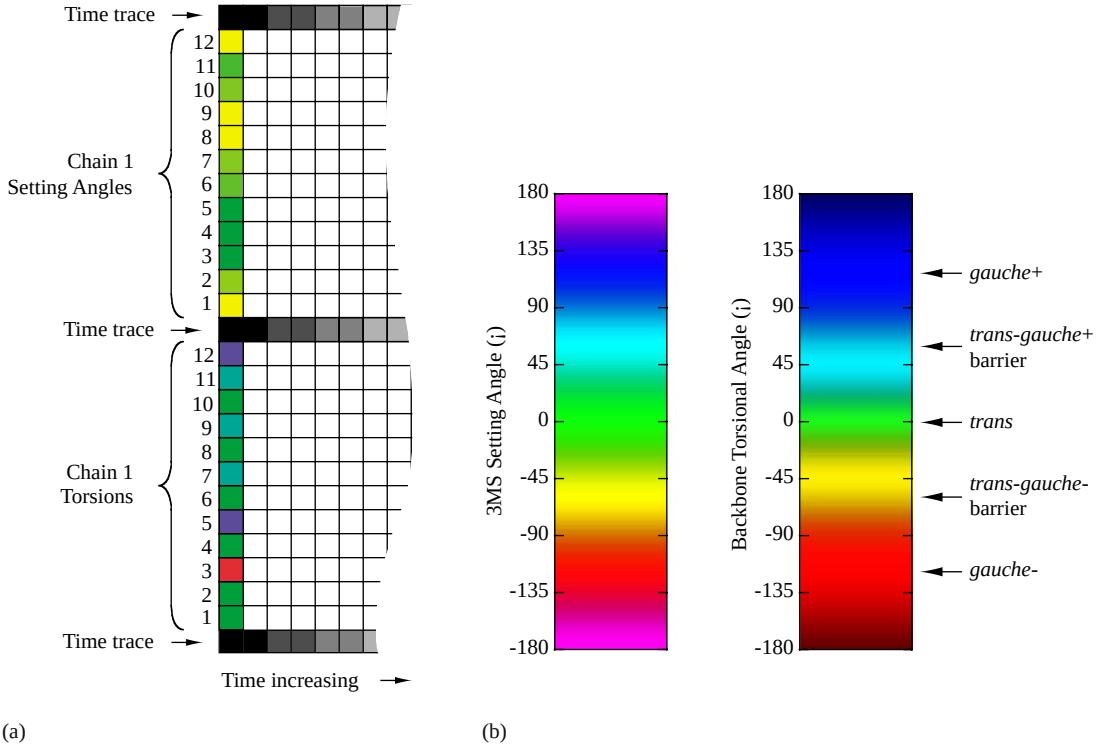

Fig. 4. (a) The method of displaying torsional angles and three-methylene-segment (3MS) setting angles as a function of time and position within a chain stem (see text). Note the use of time traces, in which each block of grey represents 2 ps. (b) The colour tables used to represent the setting angles and torsional angles.

projecting the three backbone carbon atoms onto the *x*–*y* plane and taking the angle between the bisector of the projected C_2–C_1 and C_2–C_3 bonds, and the *x*-axis, as shown in Fig. 5. The colour table for the 3MS setting angles has six different colours, each indicating a 60° range, as shown in Fig. 4(b).

When calculating the setting angles for a model, any 3MS that is tilted by more than 18° ($\cos^{-1} 0.95$) to the average *c*-axis is excluded, because the calculated setting angle then becomes unreliable. In these cases the coloured pixels are replaced by a grey scale, which is used to indicate the degree of tilt of the 3MS from the chain axis. The shades of grey associated with each angle of tilt are indicated in Fig. 6.

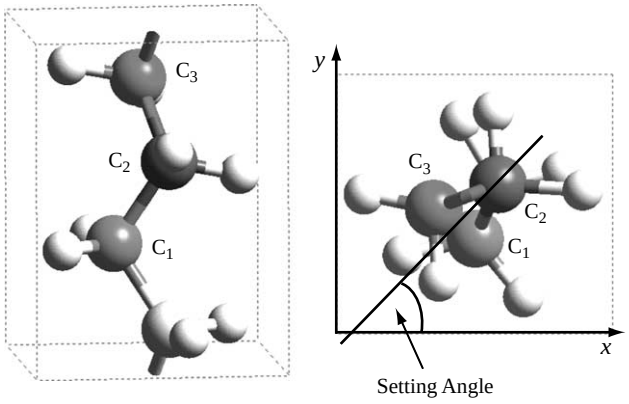

Fig. 5. Definition of a 3MS setting angle. Left: a short section of polyethylene chain with three carbon atoms labelled. The chain axis is vertical. Right: the same atoms projected onto the *x*–*y* plane. The setting angle is taken as positive when increasing in the clockwise sense.

3. Results

3.1. Lattice parameter comparison

The lattice parameters predicted from the three models at ambient pressure are shown in Fig. 7. For comparison, we also show measured lattice parameters for PE from Davis et al. [8] and Dadobaev and Slutsker [9], as well as parameters we have determined ourselves [57], and the simulated parameters of Martoňak et al. [34]. Davis et al. [8] examined a sample of commercial polyethylene with a molecular weight ($\bar{M}_n$) of 11,600 and a polydispersity of 14. Dadobaev and Slutsker do not quote a molecular weight, but specify that their crystals have thicknesses in the range 50–70 nm, and were relatively perfect. In addition we show lattice parameters for Rigidex 50

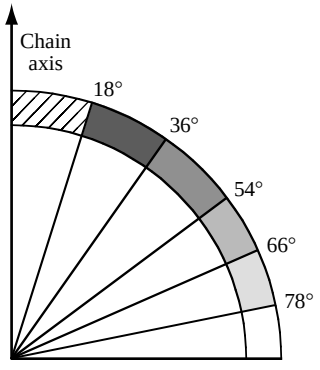

Fig. 6. The grey scales associated with the various degrees of 3MS tilt from the chain axis. Segments which are tilted by less than 18° (hatched region) are represented by the colour table shown in Fig. 4.

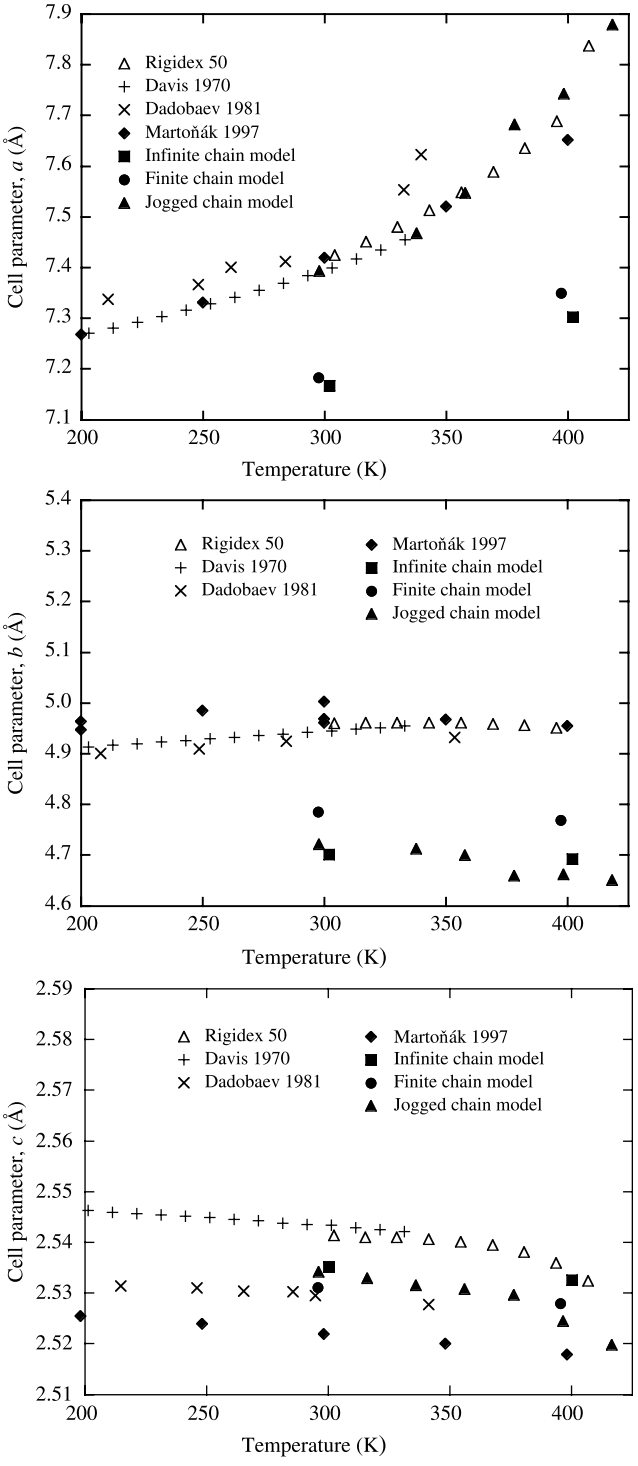

Fig. 7. The variation of the unit cell parameters *a*, *b* and *c*, with temperature for the three model systems, compared to experimental values [8,9,57] and results from previous simulations [34].

(a commercial polyethylene, with $\bar{M}_n = 7 \times 10^4$ and polydispersity of 7).

The *a* and *b* cell parameters represent an average unit cell calculated from the dimensions of the simulation box as a whole, averaged over a 10 ps sample taken towards the end of each isothermal–isobaric equilibration period, i.e. before the commencement of the NVE simulations. However, the *c* cell parameter could not generally be calculated directly from the simulation box dimensions due to the presence of chain ends. Instead it was computed from the average separation, in the *c* direction, of C_n and C_{n+2} for all the 3MS (three methyl segments) that were within a cos(0.95) (~18°) of being aligned to the average chain axis. The 'aligned segments' correspond to the *trans* sections of the alkane chains and will not include segments within the jog defects that are tilted away from the chain axis. Nevertheless, the calculation will reflect the influence of the tilted segments on their neighbours.

Because the angles of the simulation box may vary during equilibration, it is possible that the cell axes will not always be orthogonal. However, the average deviations from 90° were typically less than 1°, so the effect has been ignored. Errors in the cell parameter values were calculated as the root-mean-squared deviation from the average during the sample period. These were generally found to be smaller than the symbol plotted, and are not shown.

The changes in the cell parameters predicted by the three models are largely as might be expected from experimental results [8,9]. The thermal expansion of the crystals is manifested through large increases in the *a* parameter. In fact, the agreement between the *a* parameter from the jogged chain ($4\times6\times C_{102}$) simulation and the experimental results is surprisingly close. However, both the finite ($4\times6\times C_{48}$) and infinite ($4\times6\times24$) chain simulations fall short of this, with values about 0.2 Å too low at 300 K, and 0.3–0.4 Å too low at 400 K.

The behaviour of the *b* parameter of PE is rather more equivocal than the *a* parameter. Davis et al. and Dadobaev and Slutsker show a steady increase in *b* up to 350 K. On the other hand, our own experimental studies show that, above 350 K, the *b* parameter falls slightly. All three of the simulated models show a decrease in *b* parameter between 300 and 400 K, and the simulated values in all cases are too low by between 0.2 and 0.3 Å.

The *c* parameter of PE is generally accepted to decrease very gradually as the sample is heated, and this is borne out by all of the experimental data shown, and by all three of the models simulated. The explanation given is usually that the increasing amplitude of thermal vibrations causes the monomers to twist away from the fully extended state.

For completeness, the crystal densities of all the systems under consideration are shown in Fig. 8. As expected, the density decreases in all cases with increasing temperature. It is observed that all three computer models overestimate the crystalline density by between 5 and 9%.

The comparison of the cell parameters for the three models provides an indication of the effects that chain ends and jog defects have on the crystal packing. In the ambient structure, the presence of chain ends in the finite chain model has a negligible effect on cell parameter *a*, but a significant one on the cell parameter *b*, of the order of a one percent increase. At the higher temperature, when the chains ends can move, the finite chain model has a slightly larger *a* parameter than the infinite model. This is almost certainly due to the increased mobility facilitated by the free chain ends as the mobility

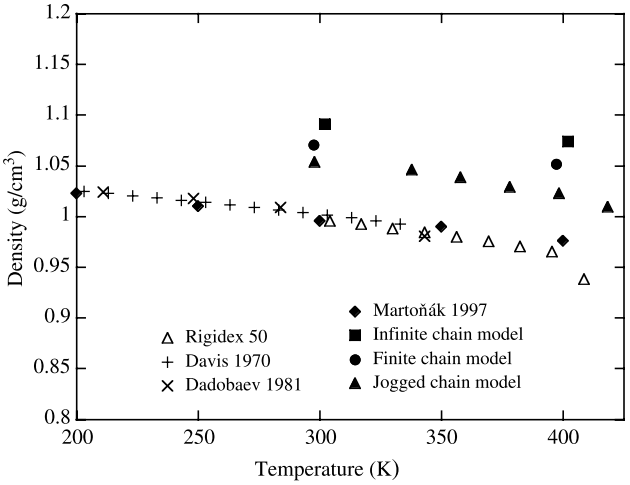

Fig. 8. The variation in density, with temperature for the three model systems, compared to experimental values [8,9,57] and results from previous simulations [34].

allows a small proportion of spontaneous *gauche* defects to form. It is also notable that the *c* parameter shows the least change with temperature for the infinite chain system, which we might again attribute to the difficulty in forming *gauche* defects when there are no free chain-ends.

The *b* parameter is too low in all three models. We attribute this to a slight error in the C–H bond length influencing the side-by-side packing density of the chains. Clearly this would need to be addressed if the model were to be used quantitatively. However in the present case, where we are mainly interested in generic behaviour, this discrepancy is not considered to be too serious.

It is most interesting to note that the high proportion of jog defects in the $4\times6\times C_{102}$ jogged chain model has such a distinct effect on the key, volume-determining cell parameter, *a*—a much larger effect than the presence of CH_3 terminal groups. This is of particular interest as there are many more conformational defects in a polyethylene crystal than chain ends [49]. It is also worth commenting that the structure of a jog defect is, in many ways, similar to that of a fold, so that the effects that both types of conformational defect have on the chain packing and particularly the setting angles might be expected to be similar. The thinnest PE lamellae observed experimentally are around 10 nm in thickness, and contain one fold per chain stem, since chain ends are rare. On the other hand, our jogged chain simulations contain one jog defect (and two chain ends) per two chain stems, but are only about 6 nm in length. Therefore, the concentration of defects in our simulations may be expected to be similar to that in a thin PE lamella, and thus, at the high end of the range expected for real PE crystals, if we accept that jogs and chain-folds are equivalent in their effect.

All three computer models show a qualitative agreement with the expected behaviour of the crystalline cell parameters and the crystal density. However, the absolute agreement is not perfect in any of the models, and they cannot be used for quantitative predictions. Nevertheless, the influence of the chain-ends and the jog defects is striking, especially given that the same force field and parameters are used in each case. The implications are clear: a computer model which aims to simulate the behaviour of PE will need to take account of the presence of defects: defects will be present in real systems and will affect the measured lattice parameters; defects in the computer models will have a similar effect. A set of molecular mechanics parameters which, when applied to a periodically bounded unit cell, successfully reproduce the cell parameters of PE, would not be capable of such good agreement in a realistic model containing a large proportion of defects.

The simulations of Martoňák et al. [34] are also included in the plots of Figs. 7 and 8. The agreement with experiment is extremely good. In fact, the work of Martoňák et al., which is based on the earlier force field of Sorensen et al. [52], makes use of an infinite chain model i.e. with the polymer chains bonded across the (001) faces of the simulation box. Thus, we might expect, from the present work, that the introduction of chain-ends and jog or fold defects, such as would be expected to occur in real crystals, would substantially worsen the agreement with experiment that those authors were able to achieve.

3.2. Torsional distributions

The distributions of torsional angles present in the models give an indication of the range of librations occurring within the *trans* potential minimum. The distributions are summarised in Fig. 9 for all three models, at 300 and 400 K. The comparison indicates that the torsional angles are the most constrained within the *trans* state for the infinite model, while the jogged chain model shows the greatest range of librations. The jogged chain model also shows two small peaks at $\pm$110–115°, which correspond to *gauche* states present within the jog (inset to Fig. 9(a)). There is a roughly equal distribution between the *gauche*$^+$ and *gauche*$^-$ states. However, there is little evidence of *gauche* defects in either the finite or infinite chain models at 300 K. Therefore we may infer that the *gauche* states in the jogged model are mainly associated with the jog itself.

On increasing the temperature to 400 K, the range of angles explored increases and the *trans* peaks broaden and reduce in height. The infinite chain model still shows no sign of *gauche* conformations. However, they are evident in the finite chain model at 400 K (inset to Fig. 9(b)), and we may presume them to be associated with the presence of chain ends. The proportion of *gauche* states in the jogged chain model also increases slightly at 400 K. However it is not possible to infer whether the addditional *gauche* states occur near the jog or the chain ends without examining the spatial distribution of torsions (see below).

3.3. Setting angle distributions

The setting angle distributions for the three models at 300 and 400 K are shown in Fig. 10. It is worth pointing out that there are actually four possible setting angles: one

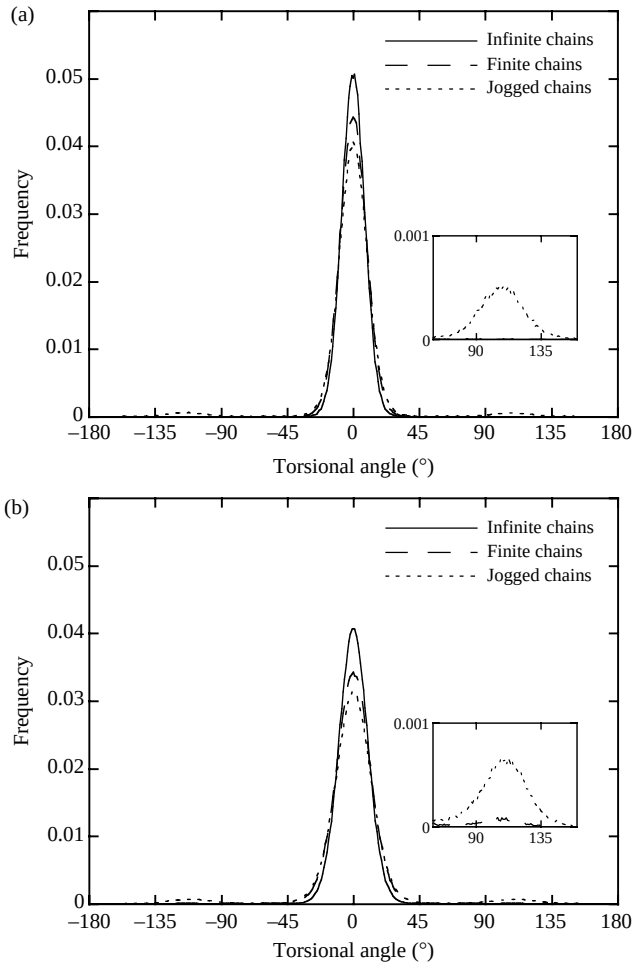

Fig. 9. The distribution of torsional angles with temperature for the three models considered: (a) 300 K and (b) 400 K.

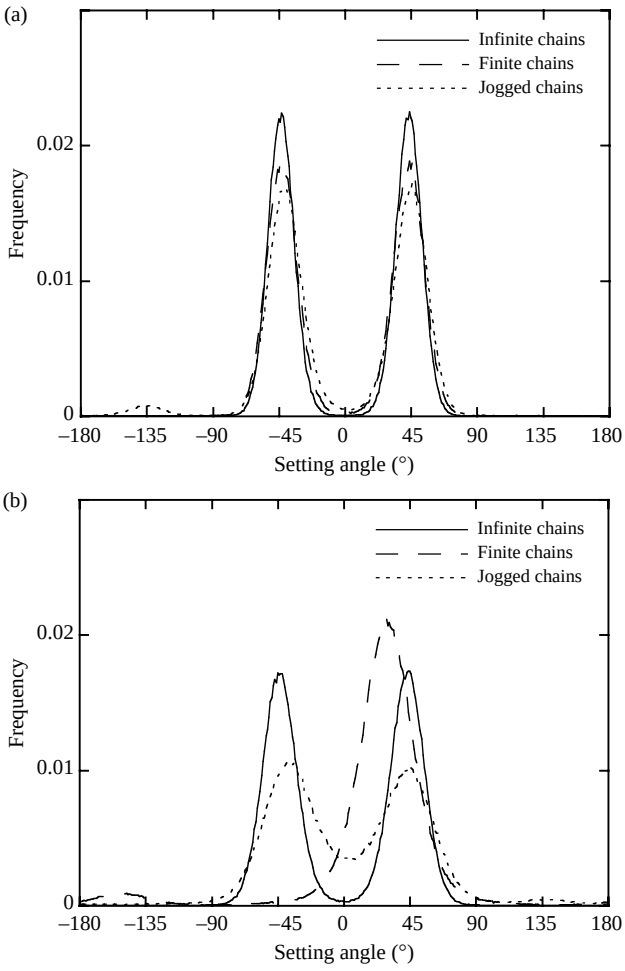

Fig. 10. The distribution of 3MS setting angles with temperature for the three models: (a) 300 K and (b) 400 K.

each for the chains at the corner and centre of the unit cell, and two more as each chain stem could be rotated through 180°. However, the symmetry seen in Fig. 10(a), dominated by two large peaks at around $\pm 45°$, is a consequence of the choice of starting configuration. The setting angles observed for all three models at 300 K are consistent with experimental figures, which are in the range 42–46° [17]. As with the torsional angles, the infinite chain model is the most ordered, and the jogged chain model is the least. The small peak at $-135°$ in the jogged chain distribution is due to certain aligned segments in the jog itself.

At 400 K the picture is somewhat different. The infinite chain model still shows two symmetrical peaks with some thermal broadening evident. However, the finite chain model appears to have undergone a transition to a state in which the planes of all the chains are parallel. On closer examination of the model, it appears that 46 of the chain stems have a setting angle at around 30°, while the other two are rotated by 180 to $-150°$. This is evidence for a transition to a monoclinic type of packing arrangement.

The distribution for the jogged chain model also shows a change at 400 K, with a marked broadening of the two peaks and a shift towards 0°. In fact, to understand the changes in the jogged model it is helpful to consider the system at intermediate temperatures (Fig. 11).

Between 200 and 360 K, there is little difference in the appearance of the distributions, apart from a gradual thermal broadening and a consequent decrease in peak height. The production run at 380 K shows a skewed distribution with more 3MS at negative setting angles than positive. From a closer examination of the model it was found that, in some of the chains only, one half of the chain on one side of the jog had rotated to the same alignment as the half on the other side of the jog. This is shown in Fig. 12. During the 400 K production run, the distributions look even again. However, this is because both halves of most of the chains (21 out of 24) are now at roughly the same setting angle on both sides of the jogs (as in Fig. 12), but half (12 out of 24) of the chains are at positive setting angles and the remainder at negative angles. The small peak at $+135°$ appears to be due to the new arrangement of the jogs. In fact, the system has separated into two domains with different orientation (Fig. 13). This separation occurs during the isobaric–isothermal equilibration period, and is then maintained for the entire production run. However, because of the small size of the model, a substantial fraction of the chains retain a herringbone arrangement with their neighbours.

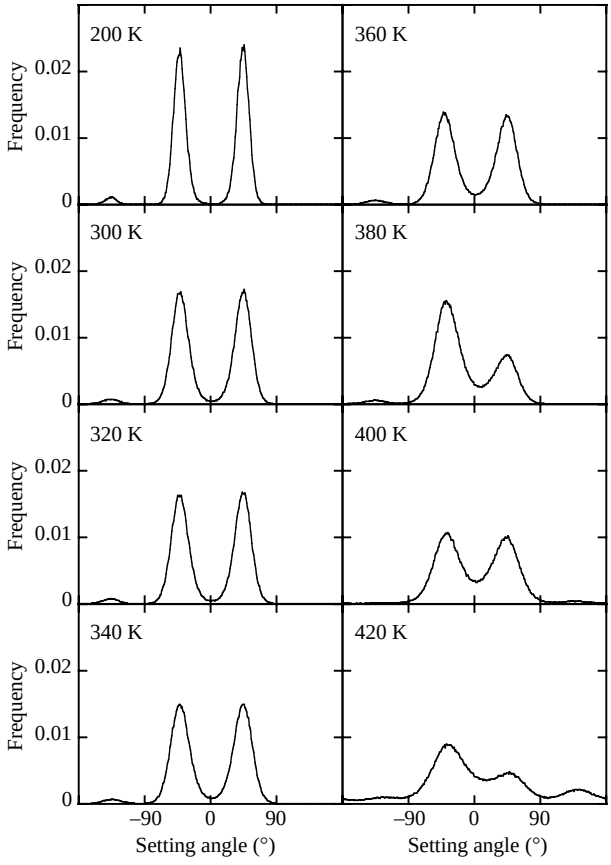

Fig. 11. The distribution of 3MS setting angles with temperature for the $4\times6\times C_{102}$ jogged chain model.

By 420 K the situation is more complicated. The two halves of the chains are rotating more frequently and occupying all four stable setting angles to some extent. In some respects, the behaviour of the model is reminiscent of that of a rotator phase, in which the molecular planes are able to rotate about the chain axis. However, in the present case, we observe a correlated rotating of domains of chains, so that locally the chains are able to retain a monoclinic type of packing. The formation of such a phase is not surprising since, at this temperature, most real systems would already have melted. In fact, the model does not quite have the correct geometry for a hexagonal phase; at 420 K $a/b=1.694$ which is less than the value of $\sqrt{3}$ required. A truly hexagonal mobile phase does occur if the model is superheated to 440 K, and this will be discussed further in a future publication [58].

3.4. Spatial distribution of 3MS

Further information concerning the onset of disorder in the $4\times6\times C_{102}$ jogged chain model may be obtained by

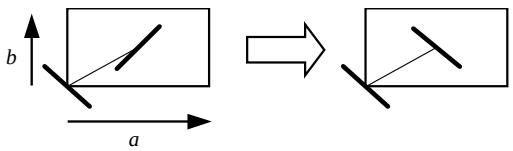

Fig. 12. The particular packing of the jogged chains that arises during the 380 K production run.

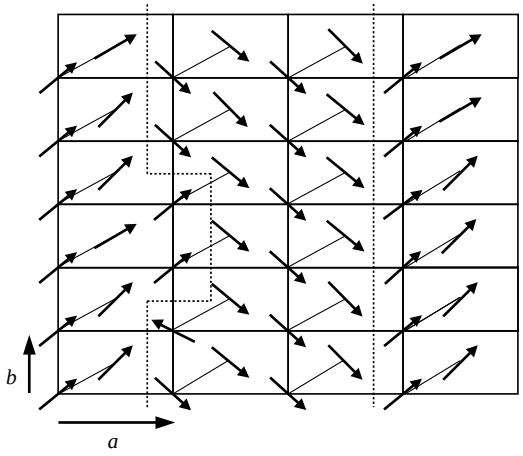

Fig. 13. A schematic of the chain-stem setting angles. The arrows point to the quadrant in which the chain-stem setting angle spends most time, during the 400 K production run. The dotted lines indicate the boundaries between the two types of packing.

examining spatial distribution functions (positional pair correlation functions) for the positions of the 3MS segments. These are calculated by taking the centre of mass of each 3MS in turn, and accumulating the relative positions of neighbouring 3MSs in an appropriate two-dimensional histogram. From these, a picture may be obtained of the spatial range and shape of the lattice vibrations within the model. Two planes have been selected for examination; the *a–b* plane normal to the chain axis and the plane containing the chain axis and the [110] direction.

Fig. 14 shows the distribution function in the *a–b* plane for several temperatures. The diffuse spots show the relative locations of the chain stems in the basal plane of the cell. The curious doubling of some spots arises due to the jogs, which cause slight displacements in the chain positions: for certain of the pair correlations, there will be contributions from two types of chain pairs, differing in which side of the jog each chain stem originates from. In practice, if we consider the correlations in the [110] direction (highlighted in Fig. 14(a)) only the odd order (i.e. the first, third, etc.) nearest neighbours suffer from the effect: for the even order neighbours, both chain stems will always fall on the same side of the jog, and a single correlation spot results.

As the temperature is increased, the distribution functions gradually become more diffuse, especially at larger separations. Above 360 K, the doublets described above merge into streaks, as the distinction between the chain stems either side of the jogs becomes blurred. Finally, at 420 K the streaks resolve into circular spots and we observe a near hexagonal, or pseudo-hexagonal, arrangement in which all chain stems are equivalent and equally spaced.

In Fig. 14(b) we observe the same transition in a plane containing the chain axis and the [110] vector. Again, as the temperature is raised, the distributions gradually blur, until at 420 K the splitting of the first and third nearest neighbour distributions is no longer evident. The plot at 420 K also indicates increased disorder parallel to the chain axis. This is

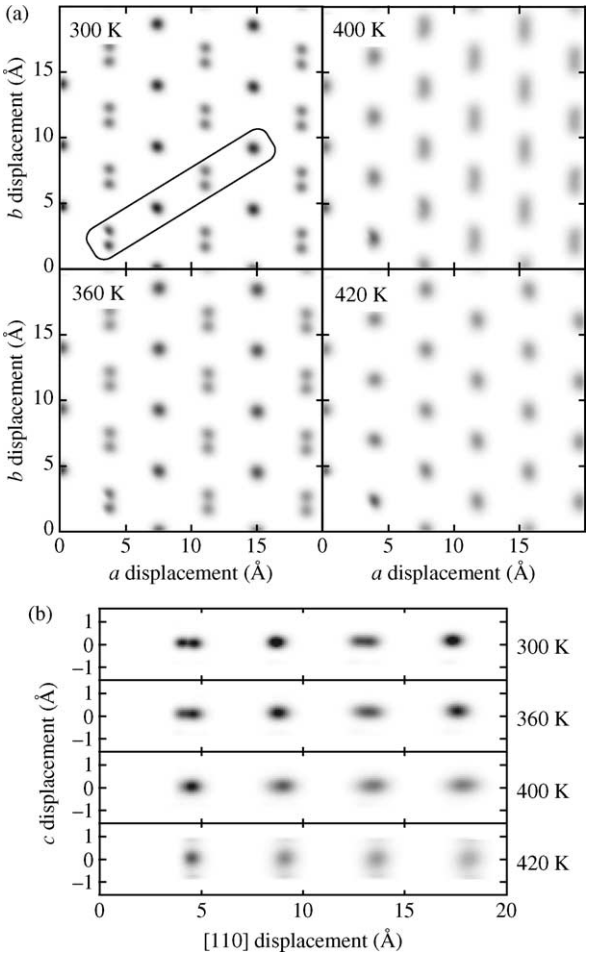

Fig. 14. (a) A plot of the averaged spatial distribution function for 3MS segments in the *a*–*b* plane. (b) A similar plot for 3MS segments in the [110] and *c*-axis directions, showing the four nearest neighbours (as highlighted in (a)).

a strong indication that chain sliding is starting to occur, which is a characteristic feature of the rotator phases in the long *n*-alkanes and, at high pressure, in PE. This feature will be explored further elsewhere [58].

3.5. Torsion and setting angle maps

While distribution functions give helpful insights into the average behaviour of a model, it is frequently necessary to examine the actual configurations of the model in order to determine its detailed behaviour. Such investigation is greatly assisted by the use of maps, which display all of the torsions and setting angles present in a chain as a function of time. The layout of the maps was described above in Section 2. The maps are particularly useful for studying the distribution and propagation of defects, as well as for demonstrating the heterogeneities within the system. Here, we will apply the maps to each model in turn.

3.5.1. Infinite chain models

Fig. 15 shows the torsional and setting angle maps for two chains taken from the infinite chain model, both at 300 and 400 K. There are several features worth noting. First,

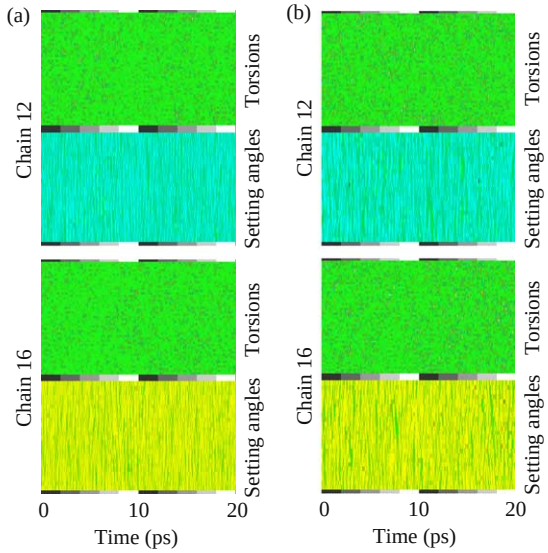

Fig. 15. The colour maps showing the torsional and setting angles for two chains (12 and 16) taken from the 4×6×24 infinite chain model during the first 20 ps of the 50 ps production runs at (a) 300 K and (b) 400 K. The colour map is defined in Fig. 4 and the chain numbers in Fig. 2.

the torsional maps are predominantly green, indicating *trans* states, with occasional pixels of yellow and cyan, which represent excursions to the *trans–gauche*$^-$ and *trans–gauche*$^+$ barriers, respectively. There are no pixels indicative of *gauche* conformations. The main difference between the maps at 300 and 400 K is that the higher temperature maps contain more yellow and cyan pixels, suggesting a greater range of librations while remaining within the *trans* potential well.

The setting angle distributions for the two chains are mainly cyan (chain 12) and yellow (chain 16). These colours reflect the fact that chain 12 has a positive setting angle, while that of chain 16 is negative, which is consistent with herringbone packing. Any green pixels present here suggest fluctuations towards 0°. The main difference between the maps at 300 and 400 K is that the latter maps are a little coarser in appearance, suggesting longer timescale correlations between the setting angles of adjacent 3MS. However, the difference is very slight, and the main observation from these maps is that there are no conformational defects present in the infinite chain simulations.

3.5.2. Finite chain models

At 300 K the maps for this model (Fig. 16) appear very similar to those of the infinite chain model. However, by 400 K the picture is totally different. During the equilibration period, the model has transformed to a state where all the chains have similar setting angles, as mentioned above. This is manifested in the fact that the setting angle distributions of both chains 12 and 16 are the same colour: predominantly cyan/green.

In addition to the change in the average setting angles of the chains there is clearly more activity in the individual setting angles and torsions. The setting angles show twist defects, starting at the chain ends and propagating into and out of the crystal. These appear as flares of yellow or dark blue, which

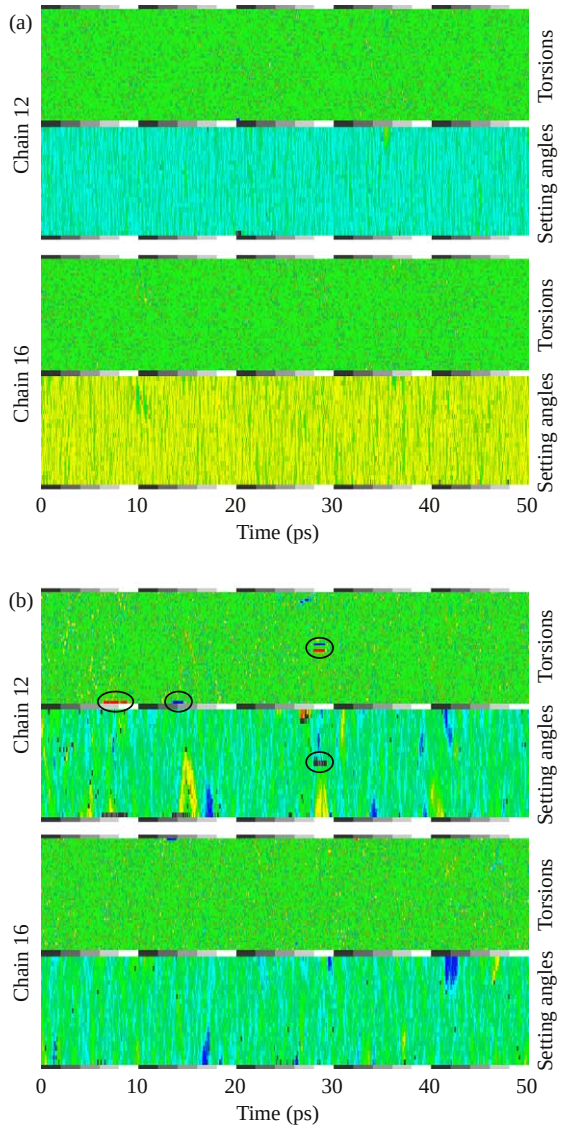

Fig. 16. The colour maps showing the torsional and setting angles for two chains (12 and 16) taken from the $4\times6\times C_{48}$ finite chain model during the 50 ps production run at (a) 300 K and (b) 400 K. The rings highlight chain-end *gauche* defects, as well as a g^-tg^+ defect. The colour map is defined in Fig. 4 and the chain numbers in Fig. 2.

correspond to rotations of $\pm90°$ away from the equilibrium setting angle. A typical lifetime of such a defect is 1–2 ps. Other shorter-lived twists also occur which are not associated with chain ends. If we examine the torsion map, the most striking feature is the presence of occasional *gauche*$^-$ (red) or *gauche*$^+$ (blue) defects at the chain ends, as well as a spontaneous *gauche*$^-$–*trans*–*gauche*$^+$ (red–green–blue; g^-tg^+) defect occurring in the middle of chain 12. This also can be seen in the setting angle map as a grey bar, because the central segment of the defect is tilted away from the chain axis by more than 18°.

3.5.3. Jogged chain models

Fig. 17 shows the behaviour of a typical chain taken from the jogged chain simulations, at four different temperatures. At 300 K the structure is relatively static and retains much of the imprint of the starting configuration of the model. The jog defect may be seen as horizontal bars of red and blue across the centre of the torsion plot, representing *gauche* defects in an otherwise *trans* (green) structure. The jog also appears as bars of grey in the setting angle plot, as these chain segments are tilted away from the chain axis by more than 18°. The jog divides the setting angle plot into two halves, coloured predominantly yellow and cyan, corresponding, respectively, to the negative and positive setting angles of the two halves of the chain. The structure of the jog defect, i.e. the sequence of *trans* and *gauche* states, clearly fluctuates during the simulation, and this is true of all of the chains in the system. The jogs are dynamic, switching frequently between conformations. For example in chain 2 (Fig. 17(a)) the structure changes more than 20 times in 50 ps. However, the most commonly observed jogs in this model consisted of two *gauche* states, separated by three or four *trans* torsions.

The 3MSs, either side of the jogs, tend to twist away from the average setting angle for that half of the chain. The effects of the twists near to the jog can be seen propagating away from the defect. This is a feature that is also visible at the bottom of the chain where persistent *gauche*$^+$ and *gauche*$^-$ defects result in the end of the chain being tilted away from the chain axis. The presence of 'end-gauche' defects have been experimentally identified by IR spectroscopy [59]. Notwithstanding the degree of fluctuation within the jogs, the overall setting angles of the chain stems remain stable, and, by reviewing the colour maps for all of the chain stems we may confirm that the familiar herringbone packing of the stems is retained.

On increasing the simulation temperature, no notable changes are observed until 360 K. At 360 K (Fig. 17(b)) two features characterise the chain behaviour. Firstly there is substantial evidence of the emergence of twisting motions propagating along the chains. Although these motions do not result in whole stem jump rotations, an emerging mechanism is evident. Secondly many of the 3MSs in the *trans* stems are more than 18° from the average chain axis, denoted by dark grey pixels, a few of which are circled in the figure. However, corresponding *gauche* defects are not observed.

At 380 K, the colour-maps reveal the onset of chain-stem rotational jumps (Fig. 17(c)). The rotation of one half of the chain, as seen after 40 ps in the illustration, has occurred in 12 of the 24 chains. A new pattern of chain packing is emerging in which many of the planar zigzags, either side of the jogs, are parallel. The structure of the jogs has also changed, with many more *gauche* defects evident.

At 400 K, there is a substantial increase in the disorder of the system, with each of the chain stems exploring a wider range of setting angles (Fig. 17(d)).

As discussed above, most of the chains have rotated so that both chain stems on either side of a jog have the same setting angle. In most cases this has occurred during the equilibration period, prior to the production run. It was the examination of these colour maps that led to the conclusions described above concerning the formation of domains (Fig. 13). Another feature of the simulations that appears at 400 K is the presence of short lived g^-tg^+ defects in the middle of the *trans* chain-stem

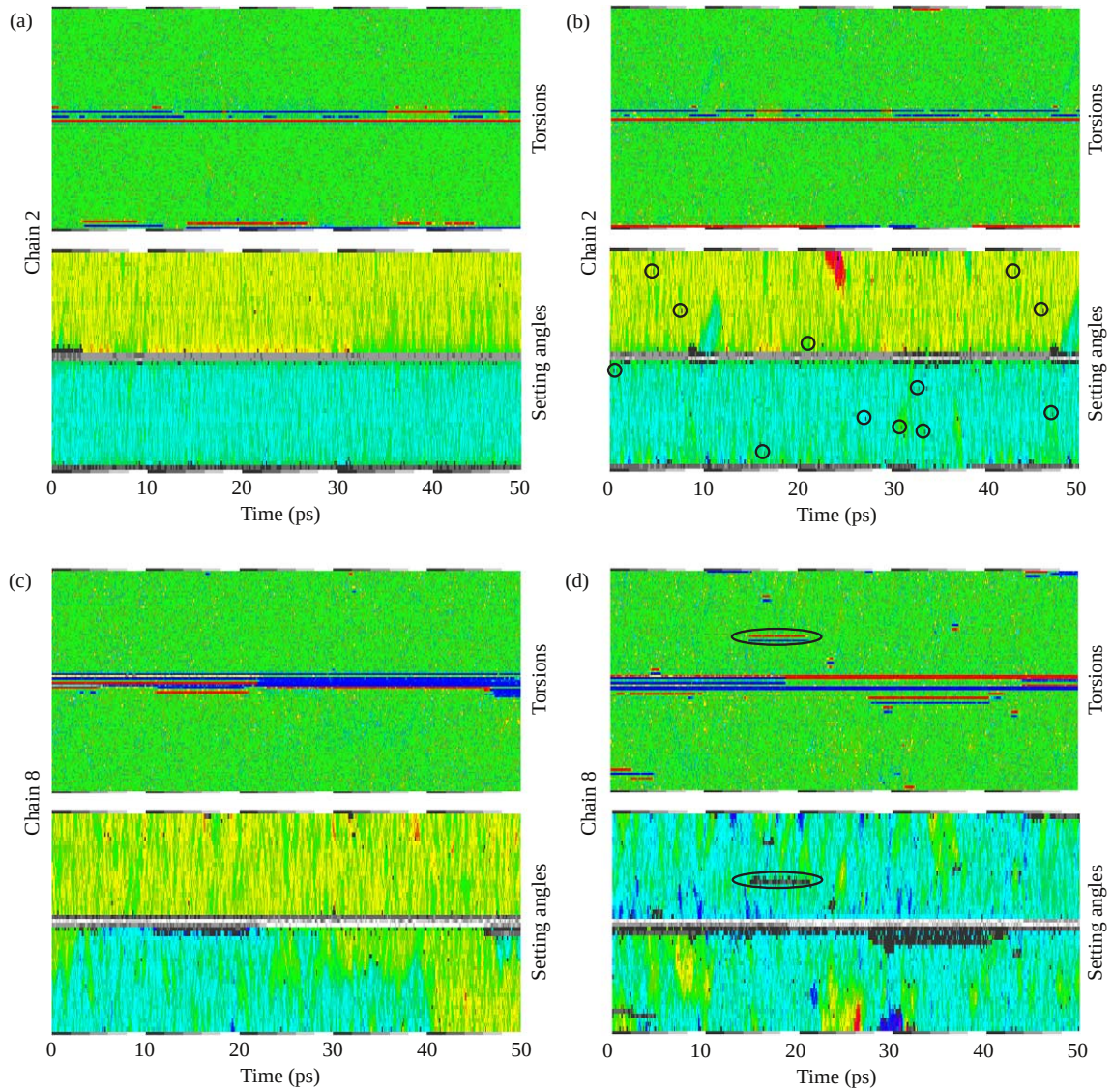

Fig. 17. The colour maps for the torsional and setting angles for a representative chain, taken from the $4\times6\times C_{102}$ jogged chain model during the 50 ps production runs at (a) 300 K, (b) 360 K, (c) 380 K and (d) 400 K. An example of a prolonged, spontaneous g^+tg^- defect, that occurs away from the jog, has been highlighted. The colour map is defined in Fig. 4 and the chain numbers in Fig. 2.

segments. These defects can have lifetimes from a pico-second upward, and result in the tilting of the corresponding 3MSs away from the chain-axis direction. One example of this is indicated in Fig. 17(d).

At 420 K, the simulation is technically above the melting point of any real system under ambient pressures. The level of disorder has increased further and rotational motions are becoming common. This is shown in Fig. 18 which shows the 3MS setting angle colour map for all of the chains in the model. The figure demonstrates the fact that the chains are undergoing a wide range of local and chain stem rotations.

3.6. Intra-chain correlations

The correlated motions of chain segments can be visualised graphically using the maps discussed above. Since the motions are very rapid it is necessary to expand the time axis by increasing the sampling frequency. This is shown in Fig. 19 for the jogged chain model at 300 K, in which particular setting angles and torsions may be observed propagating along the chains as diagonal bands of colour. The gradient of the lines corresponds to the velocity of propagation, which we estimate from the figure to be 5 km s^{-1} in these particular fluctuations. This figure seems reasonable compared with the speed of propagation of ultrasonic sound waves in highly crystalline PE (i.e. 2.43 km s^{-1}—see Ref. [60]). However, we should emphasise that the low amplitude distortions described here differ from the soliton waves described by other authors (e.g. the π and 2π twistons discussed by Zhang [61,62]) which propagate at a much lower velocity.

4. Discussion

The three models described in this paper are all proposed as suitable models for polyethylene, but each has drawbacks to

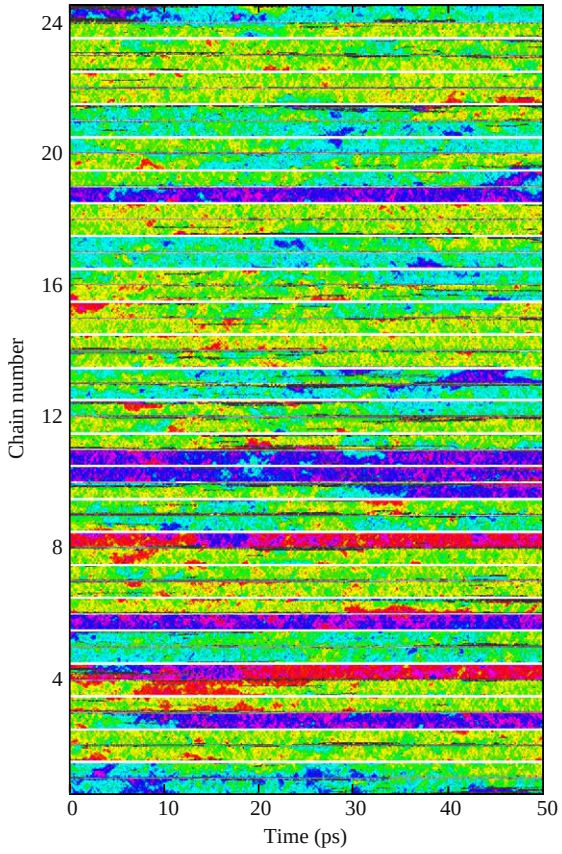

Fig. 18. The colour maps for the setting angles of all 24 chains during the 50 ps production run at 420 K. Note the substantial disorder within the system and many rotational transitions. The colour map is defined in Fig. 4 and the chain numbers in Fig. 2.

some extent, and none of the models provides a perfect fit with the crystalline unit cell parameters. The infinite chain model possesses the highest degree of order and predicts the highest density crystal. It also predicts the lowest rate of thermal expansion and the least influence of temperature on the distributions of torsions and setting angles. The model fails to display any *gauche* defects during the 50 ps simulation, but is successful in maintaining herringbone chain packing up to 400 K. On the other hand, the finite chain model, by virtue of its chain ends, does display *gauche* defects and has a less dense unit cell. Unfortunately, at 400 K the packing transforms to a monoclinic arrangement, which may possibly be related to interactions between the chain ends as these all lie in layers. The jogged chain model is the most successful in terms of matching the lattice parameters and density, and also the most interesting model in that it generates a wealth of *gauche* defects and shows the greatest differences in behaviour with temperature.

The use of jogs in this model was an artifice required to fit a long chain into a short simulation box. However, the jogs conveniently replicate the type of behaviour we might expect from chain folds and other defects (such as branch points and kinks), and so their presence within the model has a valid physical basis. We preferred not to use actual chain folds in the model because this would have produced a layered structure,

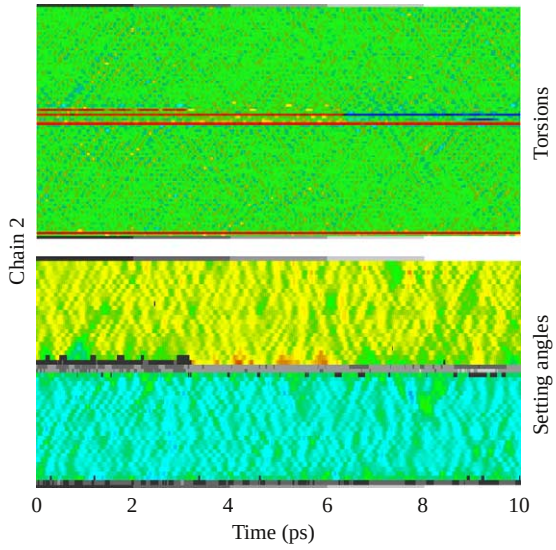

Fig. 19. The colour maps for the torsional and setting angles for chain 2 from a $4\times6\times C_{102}$ jogged chain model during a 10 ps production run at 300 K. The model was sampled every 20 fs, compared with 100 fs for the other colour maps shown above. The colour map is defined in Fig. 4 and the chain number in Fig. 2.

which would have been less realistic as a model for PE, for a number of reasons. Firstly, in the jogged chain model, the defects are distributed throughout the simulation box rather than concentrated in a plane—this provides a closer representation of the structure in the bulk of a real PE crystal, since our simulation box is too small to simulate a whole lamellar thickness. Secondly, a layer of once-folded chains would be too regular as a model for PE, but might usefully represent the long *n*-alkanes. However $C_{102}H_{206}$ only forms extended chain crystals—experimentally the chains do not fold. Also, we would be introducing another variable into the system, i.e. should all chain folds lie in one surface or be distributed randomly between the two, in which case, with such a small model, we would be concerned whether our structure was truly representative of reality. Finally, in attempting to simulate such structures, it was our experience that layers of chain-folded molecules show a much greater tendency to tilt, which was again felt to be a poor representation of real melt-crystallised PE.

It is clear that the choice of model, whether it contains infinite chains, straight chains or some other less ordered arrangement, is at least as important as the choice of force field in determining lattice parameters. This is illustrated by comparing our lattice parameter results with those of Martoňák et al. [34]. In our case, the jogged chain model provides a close match to the experimental *a* parameters, while the more ordered models underestimate the correct values by 3–6%, producing excessively dense unit cells. On the other hand, Martoňák et al. achieve a good fit to experiment using an infinite chain model that is defect free. Since real PE crystals contain many defects—the most obvious being the chain folds, but also jogs, vacancies and other types of packing error—it is clear that it will be challenging to obtain an accurate comparison between simulation and experiment unless

the same defect density can be incorporated in both. A corollary to this is that any force field which reproduces the correct crystal density of PE when applied to a perfect, defect free, model, is likely to be of limited predictive power.

Since the defect density depends on the choice of model, it is possible that two models with different force field parameters and different defect densities could have the same lattice parameters at room temperature, but would behave very differently at elevated temperature. For example, the jogged chain model produces comparable values for the *a* parameter to the model of Martoňák et al. at room temperature. However, the latter displays a hexagonal phase at 550 K, while our own jogged chain model shows a similar transformation at around 420–440 K, just above the experimental melting point. We will explore alternative models for hexagonal phases, including high pressure phases, in a subsequent paper [58].

The issue of the 'monoclinic' ordering is intriguing, and deserves further examination. It is not observed in the infinite chain model, so we believe that the problem is not intrinsic to the force field. In fact, only the finite chain model shows a definite transition to a monoclinic ordering, and this we have suggested above may be attributed to chain end interactions. At higher temperatures, the jogged chain model shows a dynamic equilibrium between regions of monoclinic and herringbone ordering. It is tempting to suggest that the jogs are promoting this behaviour, particularly given the appearance of Fig. 13, in which all but two of the chains have parallel segments on either side of the jog. This aspect of the model requires further investigation, employing larger systems and incorporating different types of defect.

If we consider each of the models discussed in the present paper, it is clear that none of them provide a fully quantitative fit to the experimental lattice parameters. However, they do display the correct qualitative behaviour and the jogged chain model, in particular, merits further consideration and development. Where there is poor agreement with experiment, we might suggest that the problems may be associated with the small size of the model and the regularity of the starting configuration and of the defects included. Further simulations with larger models will be required to confirm this.

The force field chosen for this work is, in many ways well suited to the work in hand. The force field was an evolution of a set of (mostly) non-bonded parameters intended to reproduce the crystalline structure of polyethylene, that were then tuned to provide an accurate torsional potential form. These are the two key features of the current work. Though there are later, more complex force fields tuned to reproduce vibrational frequencies and to work in mixed chemical environments, the simplicity, speed and effectiveness of the Smith and Yoon 1994 force field [51] more than justify the choice.

5. Conclusions

We have considered the behaviour of three distinctly different models for PE which contain different levels of disorder. For a given choice of force field parameters, models based on straight chain segments, whether infinite ($4\times6\times24$ unit cells) or finite ($4\times6\times C_{48}$), generate the most dense crystals, and contain the fewest defects. In particular, the infinite chain model failed to display any *gauche* defects throughout the simulations at 300 or 400 K. The closest fit to experiment was provided by a jogged chain model, consisting of 24 chains of $C_{102}H_{206}$ that passed twice through the simulation box. The jogs were required to prevent self-intersection, but effectively mimicked the influence of chain folds.

Both the finite chain model and the jogged chain model show tendencies to form regions with monoclinic-type packing at elevated temperatures. We attribute this behaviour to a combination of the small simulation box and the influence of the starting configuration. The jogged chain model also starts to undergo a transition to a hexagonal rotator phase at 420 K, slightly above the melting temperature of most polyethylenes. This phase will be examined in more detail in a future publication [58].

Finally, we note that the selection of a force field for modelling the crystal structure of polyethylene is by no means a straightforward task, and must be undertaken in conjunction with the design of the molecular model. As we have shown, the same force field can lead to very different predictions for the unit cell parameters and thermal behaviour, depending on the defects (e.g. chain ends, folds or jogs) that are present.

Acknowledgements

The authors wish to thank the H.H. Wills Physics Department, University of Bristol, and the Engineering and Physical Sciences Research Council of the UK for supporting this project through a PhD studentship. They are indebted to Dr J.K. Hobbs, Dr A.E. Terry and Dr P.J. Barham for helpful discussions concerning the experimental behaviour of PE and the long *n*-alkanes, and to Prof M.P. Allen and Prof. J.H.R. Clarke for advice on the computational methods used.

References

[1] Müller A. A further X-ray investigation of long chain compounds (*n*-hydrocarbons). Proc R Soc, A 1928;120:437–59.
[2] Bunn CW. The crystal structure of long-chain normal paraffin hydrocarbons. The 'shape' of the CH_2 group. Trans Faraday Soc 1939; 35:482–91.
[3] Kavesh S, Schultz JM. Lamellar and interlamellar structure in meltcrystallized polyethylene. 1. Degree of crystallinity, atomic positions, particle size, and lattice disorder of first and second kinds. J Polym Sci, Part A-2: Polym Phys 1970;8:243–76.
[4] Hu H, Dorset DL. Three-dimensional electron-diffraction structure-analysis of polyethylene. Acta Crystallogr 1989;B45:283–90.
[5] Bunn CW, Alcock TC. The texture of polythene. Trans Faraday Soc 1945; 41:317–25.
[6] Bunn CW. Molecular structure. In: Renfrew A, Morgan P, editors. Polythene: the technology and uses of ethylene polymers. London: Iliffe & Sons Ltd; 1957. p. 81–120.
[7] Swan PR. Polyethylene unit cell variations with temperature. J Polym Sci 1962;56:403–7.
[8] Davis GT, Eby RK, Colson JP. Thermal expansion of polyethylene unit cell: effect of lamella thickness. J Appl Phys 1970;41:4316–26.

[9] Dadobaev G, Slutsker AI. Temperature dependence of expansion of large polyethylene crystallites. Sov Phys Solid State 1981;23:1131–4.
[10] Terry AE, Phillips TL, Hobbs JK. A real-time wide-angle X-ray scattering study of crystal thickening in ultralong alkanes. Macromolecules 2003; 36:3240–4.
[11] Iohara K, Imada K, Takayanagi M. Determination of mean-square displacements of polyethylene molecules in crystal-lattice. Polym J 1972; 3:357–64.
[12] Kawaguchi A, Ohara M, Kobayashi K. Setting angle of molecular chains in polyethylene crystals. J Macromol Sci Phys 1979;B16:193–212.
[13] Kawaguchi A. Application of the optical transform to the electron-diffraction pattern of polyethylene single-crystal. Polymer 1981;22:753–61.
[14] Dorset DL, Moss B. Crystal-structure analysis of polyethylene with electron-diffraction intensity data—deconvolution of multiple-scattering effects. Polymer 1983;24:291–4.
[15] Phillips PJ, Tseng HT. The setting angle of extended chain linear polyethylene. Polymer 1985;26:650–4.
[16] Dorset DL. Electron-diffraction structure analysis of polyethylene: a direct phase determination. Macromolecules 1991;24:1175–8.
[17] Dorset DL. The setting angle of polyethylene—a critique of powder X-ray determinations. Polymer 1986;27:1349–52.
[18] Pierce RH, Tordella JP, Bryant WMD. A second crystalline modification of polyethylene. J Am Chem Soc 1952;74:282.
[19] Teare PW, Holmes DR. Extra reflections in the X-ray diffraction pattern of polyethylenes and polymethylenes. J Polym Sci 1957;24:496–9.
[20] Seto T, Hara T, Tanaka K. Phase transformation and deformation processes in orientated polyethylene. Jpn J Appl Phys 1968;7:31–41.
[21] Geil PH, Anderson FR, Wunderlich B, Arakawa TJ. Morphology of polyethylene crystallized from the melt under pressure. J Polym Sci, A 1964;2:3707–20.
[22] Bassett DC, Block S, Piermarini GJ. A high-pressure phase of polyethylene and chain-extended growth. J Appl Phys 1974;45:4146–50.
[23] Bassett DC, Turner B. On the phenomenology of chain extended crystallization in polyethylene. Philos Magn 1974;29:925–55.
[24] Sirota EB, King HE, Singer DM, Shao HH. Rotator phases of the normal alkanes: an X-ray scattering study. J Chem Phys 1993;98:5809–24.
[25] Russell KE, Wu G, Blake S, Keyding RD. ^{13}C NMR and X-ray diffraction studies of the morphology of alkanes and linear polyethylenes. Polymer 1992;33:951–7.
[26] Yamamoto T. Monte Carlo simulation of the crystal structure of the rotator phase of *n*-paraffins. J Chem Phys 1985;82:3790–4.
[27] Yamamoto T. Monte Carlo simulation of the crystal structure of the rotator phase of *n*-paraffins. II. Effects of rotation and translation of the rigid molecules. J Chem Phys 1988;89:2356–65.
[28] Fujiwara S, Sato T. Molecular dynamics simulation of structure formation of short chain molecules. J Chem Phys 1997;110:9757–64.
[29] Yamamoto T, Matsumoto S, Hirose M. A Monte Carlo study of the pattern formation during transitions in *n*-alkane crystals. J Chem Phys 2000;112:7627–33.
[30] McGann MR, Lacks DJ. Chain length effects on the thermodynamic properties of *n*-alkane crystals. J Phys Chem B 1999;103:2796–802.
[31] Mavrantza I-E, Prentzas D, Mavrantzas VG, Galiotis C. Detailed atomistic molecular-dynamics simulation of the orthorhombic phase of crystalline polyethylene and alkane crystals. J Chem Phys 2001;115: 3937–50.
[32] Ryckaert JP, Klein ML. Translational and rotational disorder in solid *n*-alkanes: constant temperature-constant pressure molecular dynamics calculations using infinitely long flexible chains. J Chem Phys 1986;85: 1613–20.
[33] Gusev AA, Zehnder MM, Suter UW. Predicting and understanding the elastic properties of polymers using atomistic simulation. Rev Inst Francais du Petrole 1986;51:131–7.
[34] Martoňák R, Paul W, Binder K. Orthorhombic phase of crystalline polyethylene: a Monte Carlo study. J Chem Phys 1997;106:8918–30.
[35] Brooke GM, Burnett S, Mohammed S, Proctor D, Whiting MC. Versatile process for the synthesis of very long chain alkanes, functionalised derivatives and some branched chain hydrocarbons. J Chem Soc, Perkin Trans 1996;(13):1635–45.
[36] Bassett DC, Olley RH, Sutton SJ, Vaughan AS. On chain conformations and spherulitic growth in monodisperse *n*-$C_{294}H_{590}$. Polymer 1996;37: 4993–7.
[37] Zeng XB, Ungar G. Lamellar structure of non-integer folded and extended long-chain *n*-alkanes by small-angle X-ray diffraction. Polymer 1998;39: 4523–33.
[38] Sumpter BG, Noid DW, Wunderlich B. Computer experiments on the internal dynamics of crystalline polyethylene: mechanistic details of conformational disorder. J Chem Phys 1990;93:6875–89.
[39] Liang GL, Noid DW, Sumpter BG, Wunderlich B. Molecular-dynamics simulations of the hexagonal structure of crystals with long methylene sequences. J Polym Sci, Part B: Polym Phys 1993;31:1909–21.
[40] Kreitmeier SN, Liang GL, Noid DW, Wunderlich B. Molecular-dynamics simulation of the temperature-dependence of lattice-parameters of alkane crystals during cooling. J Chem Soc, Faraday Trans 1995;91:2601–8.
[41] Oleinik E, Karmilov I, Shenogin S, Kalashnikov A, Mazo M, Balabaev N, et al. Computer modelling of structure and dynamics of C-50 *n*-paraffin crystal, hexagonal phase of C-50 crystal and ethylene/propylene statistical copolymers. Macromol Symp 1999;146:133–43.
[42] Mowry SW, Rutledge GC. Atomistic simulations of the α_c-relaxation in crystalline polyethylene. Macromolecules 2002;35:4539–49.
[43] Smith W, Forester TR. DL-POLY-2.0—a general-purpose parallel molecular-dynamics simulation package. J Mol Graphics 1996;14: 136–41.
[44] Berendsen HJC, Postma JPM, van Gunsteren WF, DiNola A, Haak JR. Molecular dynamics with coupling to an external bath. J Chem Phys 1984; 81:3684–90.
[45] Nosé S. A unified formulation of the constant temperature molecular dynamics methods. J Chem Phys 1984;81:511–9.
[46] Hoover WG. Canonical dynamics equilibrium phase space distribution. Phys Rev A 1985;31:1695–7.
[47] Ryckaert JP. Special geometrical constraints in the molecular-dynamics of chain molecules. Mol Phys 1985;55:549–56.
[48] Allinger NL, Chen KS, Lii JH. An improved force-field (MM4) for saturated-hydrocarbons. J Comput Chem 1996;17:642–68.
[49] Dasgupta S, Hammond WB, Goddard III WA. Crystal-structures and properties of nylon polymers from theory. J Am Chem Soc 1996;118: 12291–301.
[50] Palmo K, Krimm S. Chain elastic-modulus of polyethylene—a spectroscopically determined force-field (SDFF) study. J Polym Sci, Part B: Polym Phys 1996;34:37–45.
[51] Smith GD, Yoon DY. Equilibrium and dynamic properties of polymethylene melts from molecular dynamics simulations. I. *n*-tridecane. J Chem Phys 1994;100:649–58.
[52] Sorensen RA, Liau WB, Kesner L, Boyd RH. Prediction of polymer crystal-structures and properties—polyethylene and poly(oxymethylene). Macromolecules 1988;21:200–8.
[53] Allen MP, Tildesley DJ. Computer simulation of liquids. Oxford: Oxford Science Publications; 1987.
[54] Smith GD, Yoon DY, Jaffe RL. Long-time molecular motions and local chain dynamics in *n*-$C_{44}H_{90}$ melts by molecular-dynamics simulations. Macromolecules 1995;28:5897–905.
[55] Paul W, Yoon DY, Smith GD. An optimized united atom model for simulations of polymethylene melts. J Chem Phys 1995;103:1702–9.
[56] Doherty DC, Hopfinger AJ. Molecular modeling of polymers: molecular dynamics simulation of the rotator phase of $C_{21}H_{44}$. Phys Rev Lett 1994; 72:661–4.
[57] Lord TD, Terry AE, Hobbs AK, Kvick Å, Hanna S. In preparation.
[58] Phillips TL, Hanna S. Simulations of the mobile phases of polyethylene. Polymer, in press, doi:10.1016/j.polymer.2005.09.019.
[59] Ungar G, Organ SJ. Infra-red spectrum of tight chain folds in crystals of long linear paraffins. Polym Rep 1987;28:232–5.
[60] Hartmann B, Jarzynski J. Immersion apparatus for ultrasonic measurements in polymers. J Acoust Soc Am 1974;56:1469–77.
[61] Zhang F. 2π-twistons in crystalline polyethylene. Chem Phys Lett 1998; 293(5–6):499–502.
[62] Zhang F. Motion of twist defects in crystalline polyethylene: a molecular-dynamics study. Phys Rev B 1999;59(2):792–6.